THE JOURNAL OF PHYSICAL CHEMISTRY B

Article

pubs.acs.org/JPCB

Ostwald-Like Ripening of the Anomalous Mesoscopic Clusters in Protein Solutions

Ye Li,[†] Vassiliy Lubchenko,[‡] Maria A. Vorontsova,[†] Luis Filobelo,[†] and Peter G. Vekilov*[,†,‡]

[†]Department of Chemical and Biomolecular Engineering, and [‡]Department of Chemistry, University of Houston, Houston, Texas 77204, United States

Supporting Information

ABSTRACT: Metastable clusters of mesoscopic dimensions composed of protein-rich liquid exist in protein solutions, both in the homogeneous region of the solution phase diagram and in the region supersaturated with respect to an ordered solid phase, such as crystals; in the latter region they are crucial nucleation sites for ordered solids. We monitor, using three optical techniques, the long-term evolution of the clusters in lysozyme solutions at conditions where no condensed phases, liquid or solid, are stable or present as long-lived metastable domains. We show that cluster formation is a reversible process and that the clusters are in near equilibrium with the solution, up to a capillary correction. In contrast to classical phase transformations, the solution concentration at cluster−solution equilibrium is close to its initial value; this is akin to chemical reaction equilibria and demonstrates the complex chemical composition of the clusters. However, similar to classical phase transformations, en route to full equilibration, the average cluster size grows with time following a universal law $t^{0.26\pm0.03}$, independent of the cluster volume fraction; the cluster size distribution is scale-invariant at all stages of cluster evolution. Despite the correspondence of these behaviors to the Lifshitz−Slyozov−Wagner (LSW) theory predictions, the cluster sizes are about 10× smaller than the LSW prediction, likely due to the complex cluster composition. The observed cluster evolution helps us to understand nucleation mysteries, such as nucleation rates lower by orders of magnitude than classical theory predictions, nucleation rate variable under steady conditions, and others.

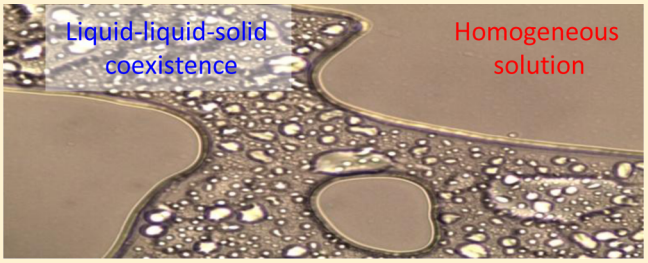

INTRODUCTION

Clusters of protein-rich liquid have been detected in solutions of several proteins: lumazine synthase,[1,2] oxy- and deoxyhemoglobins A and S,[3−5] lysozyme,[6,7] and others, at electrolyte concentrations ranging from 20 mM[7] to 1.3 M,[1,2] by atomic force microscopy,[1] dynamic light scattering,[2,3,6,7] and UV resonance Raman spectroscopy.[5] The clusters are mesoscopic in size, from under one hundred to several hundred nanometers,[2−4,7] and liquid in nature.[2,3,8] The clusters occupy a low fraction of the solution volume: from $\sim10^{-7}$ (below which they are not reliably detectable) to $\sim10^{-3}$. The cluster volume fraction remains at these low levels even as the protein concentration in the bulk solution approaches that of the liquid within the clusters.[4,7] The mesoscopic clusters exist with similar characteristics both in the homogeneous region of the phase diagram of the protein solution (where no condensed phases, liquid or solid, are stable or present as long-lived metastable domains) and under conditions supersaturated with respect to ordered solid phases, such as crystals[2] or sickle cell hemoglobin polymers.[3,9] In supersaturated solutions the clusters are crucial sites for the nucleation of ordered solid phases.[9−11] The protein clusters are similar to, but larger than, clusters found in solutions of biominerals,[12−14] organic molecules,[15,16] polymers,[17] and colloids,[18−20] where they also play a crucial role in crystal nucleation.

The anomalous mesoscopic clusters are of interest because their existence challenges our understanding of phases and phase equilibria. Furthermore, insight into cluster behavior may provide means to control nucleation, one of the most secretive processes in chemistry and materials science. Recent studies reveal that the small fraction of protein contained in the clusters reflect the significant free energy cost of increasing the protein concentration: the chemical potential of the protein in the clusters is higher by $\sim10k_BT$ than that in the solution.[7] The mesoscopic size of the clusters is significantly greater than the predictions of several mechanisms of cluster formation in protein and colloid solutions.[7,21] If these mechanisms are inactive, due to the free energy excess of high concentration protein liquid, the clusters should consist of just a few protein molecules, as indicated by a straightforward thermodynamic evaluation.[7] To solve the puzzle of the cluster size, we argued in ref 7 that the clusters largely consisted of transient protein complexes that formed at high protein concentrations; this mechanism is illustrated in Figure 1. Within this mechanism, the cluster size R_{cl} is determined not by the stability of the protein-rich liquid but by the diffusivity D and lifetime $\tau_{complex}$

Received: April 6, 2012
Revised: August 8, 2012
Published: August 13, 2012

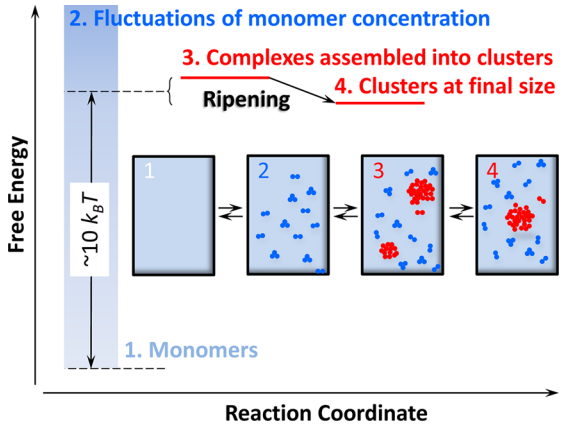

Figure 1. Free energy variation along the reaction coordinate for formation of the anomalous mesoscopic clusters, steps 1−3, discussed in ref 7, and their ripening, the transition from 3 to 4, discussed here. Insets: schematic illustrations of the four steps of the cluster formation mechanism. Color indicates chemical nature of species: blue, monomers; red, complexes.

of the transient complexes: $R_{cl} = (D\tau_{complex})^{1/2}$ ref 7. Several types of interactions, hydration, electrostatic, and the formation of domain-swapped dimers after partial protein unfolding, were considered and tested as possible bonds between the protein molecules in the transient complexes.[7]

Here we report another intriguing behavior of these anomalous clusters: their size increases following a universal power law, independent of the protein concentration and cluster volume fraction. The cluster size distribution retains a scale-invariant shape during their evolution. We highlight the similarities and differences of these results with the predictions of the Lifshitz−Slyozov−Wagner (LSW)[22,23] law of Ostwald ripening,[24] i.e., coarsening of the domains of a newly nucleated phase driven by minimization of the surface free energy.

EXPERIMENTAL METHODS

Solution Preparation. All experiments reported here were carried out with the protein lysozyme. It offers the advantage of ready availability as a highly purified preparation[25] (from Seikagaku, Japan, 6× crystallized), an extensive database of known physicochemical properties, and robustness allowing for data collection over many hours and quantitative reproducibility of independently performed experiments. In most experiments lysozyme solutions were prepared by dissolving the freeze-dried commercial lysozyme preparation without additional purification in 20 mM Na-HEPES (*N*-2-hydroxyethylpiperazine-*N*′-2-ethanesulfonic) buffer at pH 7.8. The ionic strength in this buffer is ∼30 mM, due to dissociation of the amino and sulfonic groups of HEPES. Furthermore, the commercial lysozyme preparation contains ∼8 mol Cl^-/mol lysozyme. If all Cl^- ions are released upon dissolution, the ionic strength would increase form that of the buffer to ∼85 mM in a 100 mg mL^{-1} M lysozyme solution and to ∼140 mM in a 200 mg mL^{-1} solution. All experiments were carried out at 22 °C. Cluster behavior was monitored at concentrations 85, 100, 150, and 200 mg mL^{-1}. Even at the highest concentration, the solutions are stable and clear for several weeks, with no crystallization, liquid−liquid separation, or other aggregation occurring. In one series of experiments, in which the light scattering signature of liquid−liquid separation was compared to that of the metastable clusters, lysozyme was dissolved in

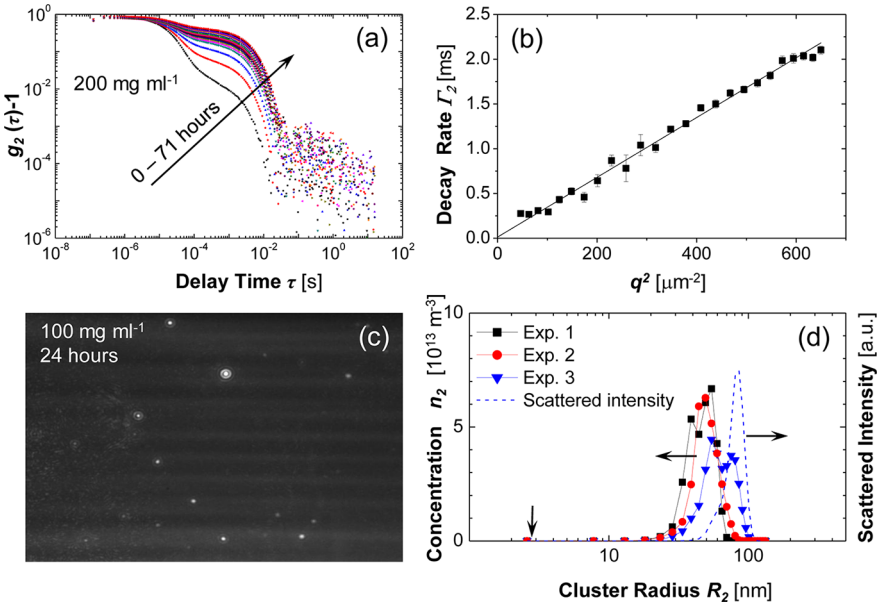

Figure 2. Identification and characterization of clusters in lysozyme solutions. (a and b) By dynamic light scattering in a solution with protein concentration as shown in (a). (a) The intensity correlation functions $g_2(\tau)$ recorded at 90° at times ranging between 1 and 71 h after solution preparation and filtering. All correlation functions reveal the presence of two scatterers: lysozyme monomers with characteristic diffusion time $\tau_1 \approx 20$ μs, and the clusters with $\tau_2 \approx 10$ ms. (b) The dependence of the decay rate of the intensity scattered from clusters $\Gamma_2 = \tau_2^{-1}$ on the scattering vector q. (c and d) By Brownian microscopy, in a solution with concentration shown in (c), 24 h after the solution was prepared and filtered. (c) A snapshot from the movie from which the cluster Brownian trajectories are determined, showing several clusters detected from the light that they scatter; the monitored volume is 120 × 80 × 5 μm^3. (d) Three independent distributions of the number concentration of clusters on their size. The expected distribution of intensity scattered from such a cluster population according to the Rayleigh law is shown. Vertical arrow indicates the size of the monomers. Horizontal arrows refer respective data sets to left and right ordinate axes.

dx.doi.org/10.1021/jp303316s | J. Phys. Chem. B 2012, 116, 10657−10664

0.05 M Na-acetate buffer at pH 4.50 in the presence of 4% (*w*/*v*) NaCl, prepared as discussed in refs 26−29.

Dynamic Light Scattering (DLS) from Protein Solutions. Dynamic light scattering data were collected with an ALV goniometer equipped with He−Ne laser (632.8 nm) and ALV-5000/EPP Multiple tau Digital Correlator (ALV-GmbH, Langen, Germany). Prior to loading in the cuvette, the solutions were filtered through 0.22 μm Millipore filters. Unless specified otherwise, intensity correlation functions were acquired for 60 s at 90°; for definitions and further details, see ref 3. We note that lysozyme solutions are completely transparent at 632.8 nm, making DLS a convenient structural probe even at the high protein concentrations employed in this work.

Static Light Scattering (SLS) Characterization of the Osmotic Compressibility. The osmotic compressibility was measured by static light scattering (SLS) using the same ALV device used for DLS, at the same concentrations at which the clustering behavior was monitored. Static light scattering outputs the ratio KC_1/R_θ, where C_1 is the protein concentration, $R_\theta = I_\theta/I_0$ is the Rayleigh ratio of the intensity of the light scattered at angle θ to the incident intensity, K is a system constant defined as $K = N_A^{-1}(2\pi n_o/\lambda^2)^2(dn/dC_1)^2$,[30] N_A is the Avogadro number, n is the solution refractive index, and $n_0 = 1.331$ is the refractive index of the solvent at the wavelength of the laser beam λ.[31] Determinations of dn/dC_1 were carried out using a Brookhaven Instruments differential refractometer operating at a wavelength of 620 nm.[2,32]

The KC_1/R_θ ratio is proportional to the osmotic compressibility $(KC_1/R_\theta) = (1/RT)(\partial\Pi)/\partial C_1)$, where Π is the contribution of the scattering species to the osmotic pressure of the solution, R is the universal gas constant, and T is the absolute temperature.

The osmotic compressibility allows evaluation of the protein chemical potential μ_1 by the relation[28] $\mu_1 = \int(\partial\Pi)/\partial C_1))(M_w/C_1)\, dC_1$, where M_w is the protein molecular mass. The relation between the KC_1/R_θ ratio and the protein chemical potential μ_1 indicates that an increase in KC_1/R_θ at fixed protein concentration, solution composition and temperature reflects an increase in μ_1 and vice versa: decrease in KC_1/R_θ reflects a decrease in μ_1.

Brownian Microscopy. We use a Nanosight LM10-HS device optimized for determination of protein aggregates. The protein solution, held in a custom-made cuvette, is illuminated by a specially configured laser beam. Data are collected from a solution volume 120 × 80 × 5 μm^3 (width × length × height). This device detects the light scattered off the clusters by a camera attached to a microscope. Since the protein molecules are significantly smaller than the clusters, the light scattered from them is insignificant even at relatively high protein concentrations. Each cluster is treated as a point source of scattered light and its location is determined from images such as the one in Figure 2c. The Brownian trajectories of the clusters are tracked by comparing the locations of the individual clusters in a sequence of images collected at a rate 30 s^{-1}. The diffusion coefficients of the individual clusters are computed from the trajectories indicative of regular Brownian motion of the imaged cluster. The clusters sizes are determined using the Einstein−Stokes relation and the solution viscosity determined as discussed below. The results are output as concentration of clusters of certain size as a function of this size.

The method was tested by a solution of latex spheres of radius 300 nm in water and found to faithfully reproduce the particle size and concentration.

RESULTS AND DISCUSSION

Cluster Evolution. We monitor over three days the cluster evolution in lysozyme solutions with concentrations 85, 150, and 200 mg mL^{-1} in 20 mM HEPES buffer with pH 7.8 at 22 °C using dynamic light scattering (DLS). Solutions with these compositions are homogeneous (i.e., no condensed phases are stable or present as long-lived metastable domains) at temperatures from −1 °C, below which the solution freezes, to ∼40 °C, above which the protein may denature; the absence of macroscopic protein condensed phases simplifies monitoring and understanding of cluster behaviors.

The autocorrelation function of the scattered light in Figure 2a has two distinct shoulders. We use a combination of a commercially available inverse-Laplace transform algorithm[33] and two newly developed models,[34] to determine the diffusion time distribution of the scatterers. The resulting distributions are bimodal. A computation of a diffusion coefficient from the scattering vector $q = 18.7 \times 10^6$ m^{-1} and the characteristic time $\tau_1 \approx 25$ μs of the short-time peak yields $D_1 = (q^2\tau_1)^{-1} = 1.1 \times 10^{-10}$ m^2 s^{-1}, near the value for lysozyme;[35,36] hence, this peak is assigned to individual protein molecules. The q dependence of the center of the long-time peak, shown in Figure 2b, indicates the presence of a relatively monodisperse population of diffusing species that are $\sim 10^2$ times larger than that of the protein molecules; we assign this peak to the clusters.[7] Consistent with this monodispersity, the autocorrelation functions are fitted well by intensity and cluster size distributions with widths ranging from 0 to ∼50% of the peak center. From the cluster−peak center in the intensity distribution function, we determine the average cluster size using the Einstein−Stokes relation and independently measured viscosity.[3,34]

We independently verify the presence, size, polydispersity, and concentration of the clusters by Brownian microscopy,[37] whereby individual clusters are directly detected and counted, as in Figure 2c, and their Brownian trajectories are monitored. The diffusion coefficient of each cluster is extracted from its trajectory and, via the Einstein−Stokes relation and independently measured solution viscosity, is used to determine its size. Note that this determination does not rely on the value of the scattered intensity. The resulting size distribution, shown in Figure 2d, is relatively symmetric and narrow: the cluster radii vary from 30 to 90 nm, with a mean at about 60 nm. This distribution, measured at 24 h, is similar to the DLS-inferred distribution at the same solution age after one corrects the latter distribution to account for the Rayleigh law: According to this law, the scattered intensity is proportional to the sixth power of cluster size.[3,34] The Brownian microscopy-produced distribution, multiplied by R^6 is shown in Figure 2d; it exhibits a maximum at ∼100 nm, in agreement with Figure 3a at 24 h. Because of the Rayleigh correction, the DLS-inferred cluster radius is overestimated by about 1.6; this factor is time-independent.

Figure 3a demonstrates that the determination of the cluster size from light-scattering data is robust with respect to the methods of fitting of the correlation function. Importantly, we see that the cluster size does not depend on the monomer concentration in the solution. At the three examined concentrations, the mean cluster size increases over 71 h

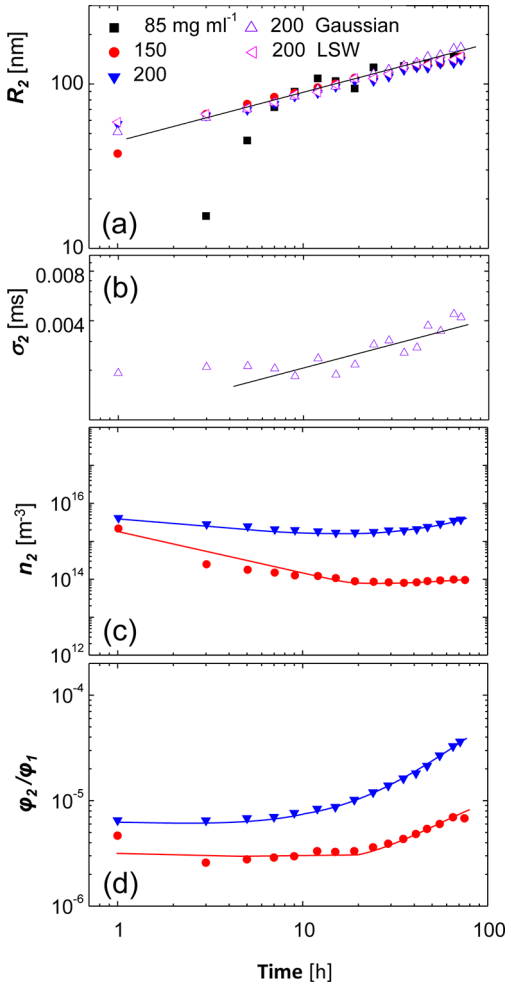

Figure 3. Evolution over 71 h of cluster population characteristics at three concentration indicated in (a). Time is measured form the moment of solution preparation and filtering. (a) The average cluster size R_2 determined by fitting the cluster part of the intensity distribution function with the Dirac delta function (solid symbols), or with a Gaussian function and the Lifshitz–Slyozov–Wagner (LSW) scale-invariant function, in which the width of the cluster size distribution is determined by the mean cluster radius (open symbols). Straight line corresponds to relation $R_2 = 5.6 \times 10^{-9}\ t^{0.26}$ m. (b) The width of the cluster peak σ_2 in the distribution function determined from the Gaussian fits. Straight line has the same slope as the line in (a). (c) Number concentration of clusters n_2. (d) The ratio of the cluster volume fraction to that of the monomer φ_2/φ_1. $\varphi_1 = C_1/\rho_1$, where ρ_1 = 1.18 g cm^{-3} [39] is the mass density in the lysozyme molecules, so that $\varphi_1 = 0.137$ at C_1 = 150 mg mL^{-1} and 0.170 at 200 mg mL^{-1}. Straight lines through data for 150 mg mL^{-1} for $t \leq 20$ h have slope −1 in (c) and 0 in (d); the extensions of these lines for $t >$ 20 h are guides for the eye. Lines through data for 200 mg mL^{-1} in (c) and (d) are just guides for the eye. R_2, σ_2, n_2, and φ_2 were determined from the correlation functions g_2 such as those in Figure 2a as discussed in the Supporting Information; n_2 and φ_2 were calculated from the fits with the Dirac delta function.

from ∼50 to ∼180 nm, following a power law $R_2 = (5.6 \pm 0.3)10^{-9}(t/\mathrm{s})^{0.26\pm0.03}$ m. In the 85 mg mL^{-1} data set, the point at t = 1 h is not shown because of its high uncertainty; the data points at 3 and 5 h might indicate nonsteady state coarsening until the steady growth regime is reached at longer times, as seen before.[38] The scatter of this data set at times between 7 and 22 h is likely due to low cluster volume fraction at this concentration, as discussed in ref 3.

Are the Clusters Domains of a Stable Phase? The observed evolution of the cluster size is in apparent contradiction with the main result of the model illustrated in Figure 1, which predicts that the clusters are constrained to a mesoscopic R_{cl} defined above.[7] The size evolution in Figure 3a allows the possibility that the objects monitored in Figures 2 and 3 are not mesoscopic clusters but domains of a stable phase slowly evolving toward a macroscopic final size. Several experimental observations refute this scenario:

First, the protein volume fraction $\varphi_1 = C_1/\rho_1$, where ρ_1 = 1.18 g cm^{-3} from ref 39 is the mass density in the lysozyme molecules, is $\varphi_1 = 0.137$ at C_1 = 150 mg mL^{-1} and $\varphi_1 = 0.170$ at 200 mg mL^{-1}. Since at C_1 = 150 mg mL^{-1} the cluster volume fraction is only $\varphi_2 \approx 4 \times 10^{-7}$, cluster formation does not lower the solution concentration. This volume fraction is steady for 20 h, Figure 3d, so a hypothetical stable cluster phase would be in near-perfect equilibrium with a solution of that C_1. Then, cluster formation in solution with initial protein concentration C_1 = 200 mg mL^{-1} would bring down C_1 to the same value at the cluster–solution equilibrium. As a result, φ_2 would increase by $\Delta\varphi_2 = \Delta C_1/C_2 \approx 0.11$, where C_2, reasonably assumed to be ∼450 mg mL^{-1}, is the protein concentration in a hypothetical stable cluster phase. The resulting φ_2 would correspond to a macroscopic phase separation. No such separation is observed at C_1 = 200 mg mL^{-1}. The steady value $\varphi_2 \approx 1.2 \times 10^{-6}$ is about five orders less than the above estimate. At long times in Figure 3d, it evolves to 6.8×10^{-6}; this evolution of φ_2 is discussed below.

Second, as discussed above, no stable phases, liquid or solid, exist in solutions of the tested compositions: solutions with the three tested concentrations were kept at 22 °C for up to 30 days, loaded in microscope slides, and examined under bright-field and differential interference contrast (DIC) microscopies; the latter method is sensitive to elongated objects such as potential amyloid fibrils. All microscopy observations revealed homogeneous solutions with no liquid or solid formations; occasional air bubbles of sizes around 10 μm were likely introduced during the solution transfer to the slide. Even though amyloid fibrils or proto-fibrils have been observed in lysozyme solutions only at temperatures above 30 °C,[40] they may have formed in our long duration experiments. To test for the presence of amyloid structures with sizes below the detection limit of DIC microscopy, we applied the dye Thioflavin T to the aged solutions: this dye forms a complex with amyloid aggregates which fluoresces under UV illumination. While the Thioflavin T assay shows the presence of amyloid structures at $T >$ 34 °C,[41] no fluorescence was detected from the solutions tested here.

Third, the clusters are constrained to their mesoscopic sizes and extremely low volume fractions even after extended periods of equilibration with the solution. Figure 4a displays the correlation functions from a solution similar to those analyzed in Figures 2 and 3 at 656 h after solution preparation. This function is similar to those in Figure 2a, but it reveals a ∼ 3× slower diffusion of the clusters. To understand this slowing down, we monitored in parallel the dynamics of latex spheres of radius 200 nm suspended at volume fraction 10^{-5} in an identical solution. The correlation functions from the solutions with the suspended spheres, illustrated in Figure 4b, indicate that the solution viscosity has increased by ∼3×, from 1.45[34] to 4.5 mPa s. The characteristic diffusion time of the spheres in Figure 4b is similar to that of the clusters in Figure 4a, hence, the cluster radius is about 200 nm. Using this radius, we

dx.doi.org/10.1021/jp303316s | J. Phys. Chem. B 2012, 116, 10657–10664

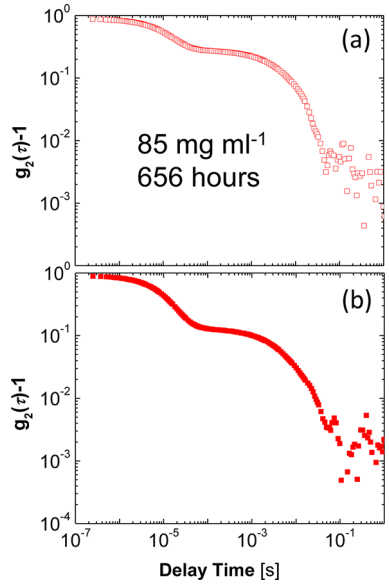

Figure 4. Intensity correlation functions from: (a) A lysozyme solution with shown concentration at shown time after solution preparation; shoulder with characteristic τ_1 = 20 μs corresponds to lysozyme monomers and shoulder with τ_2 = 26 ms to clusters. (b) An identical solution containing latex spheres with $R_{spheres}$ = 200 μm occupying volume fraction $\varphi_{spheres} = 10^{-5}$ at same time after solution preparation; shoulder at τ_1 = 20 μs corresponds to lysozyme monomers and shoulder at τ_2 = 30 ms to the latex spheres. Since the spheres scatter light significantly better than the clusters, light scattered from the clusters is not detected.

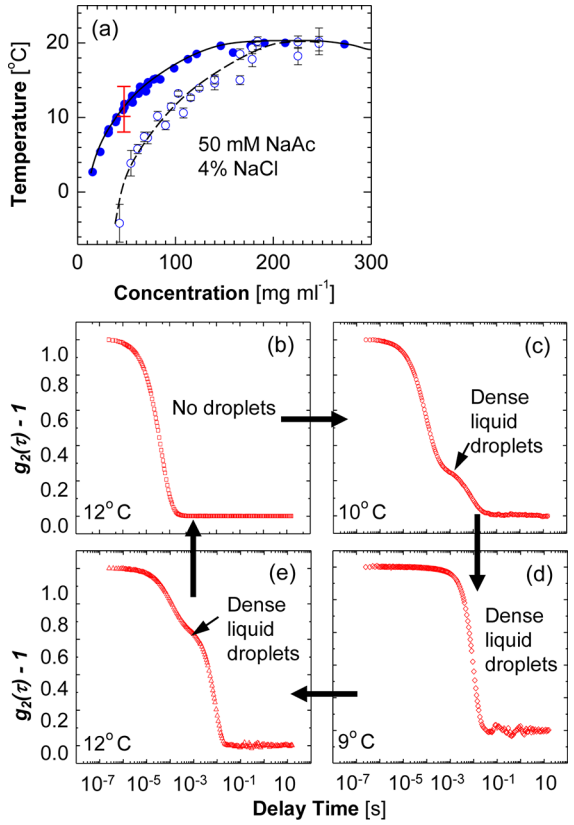

Figure 5. Light scattering signature of liquid–liquid (L-L) separation in a lysozyme solution in 0.05 M Na-acetate buffer, pH 4.50, containing 4% (*w*/*v*) NaCl. (a) The phase lines characterizing L-L separation: solid symbols denote the coexistence line, open symbols—the spinodal, data from ref 28. Vertical bar indicates concentration of tests in (b–e); horizontal bars, of three chosen temperatures. (b–e) The intensity correlation functions $g_2(\tau)$ recorded at 90° at the temperatures indicated in each panel. Arrows between panels indicate directions of temperature changes. Temperature was held steady at each setting for 15 min. The cycle was repeated several times with identical observations. No clusters or droplets are present above the L-L coexistence line at this solution composition, as seen in (b).

determine the cluster volume fraction form the intensity scattered by them as in refs 3 and 34, and we get $\varphi_2 \approx 2 \times 10^{-6}$.

Forth, if the clusters consisted of a stable dense liquid, their size and volume fraction would increase dramatically faster. Since no liquid–liquid (L-L) phase separation occurs in the studied HEPES solution, to test this point we monitor the L-L separation in solutions containing 4% NaCl in 50 mM Na acetate buffer. For the chosen composition, the phase lines characterizing the L-L transformations, Figure 5a, are known with high accuracy.[28,42] At the chosen protein concentration of 48 mg mL^{-1}, marked with a vertical line in Figure 5a, the L-L binodal is at 10.5 °C. At 12 °C, this solution is homogeneous, and the correlation function in Figure 5b reveals the presence of a single scatterer with a diffusion time ~20 μs: the lysozyme monomer. Clusters, if present, maybe at volume fraction below the detection limit due to the low protein concentration. At 10 °C, just below the L-L binodal, Figure 5c, large scatterers appear and the intensity scattered from them grows in time. After 15 min at 10 °C, temperature was lowered to 9 °C, further below the L-L binodal, and kept at this value for another 15 min, Figure 5d. The shoulder corresponding to the large scatterers grows fast and overpowers the scattering from the monomers; their size grows to 1.4 μm. We conclude that the large scatterers are droplets of the dense liquid, which is stable with respect to the solution. (Note that the dense liquid is metastable with respect to the crystals, which would form under these conditions after about 2 days;[43] the phase lines of the solution-crystal equilibrium are not shown in Figure 5a and can be seen in, e.g., ref 7). The fast nucleation and growth of the droplets of stable dense liquid is consistent with previous microscopy observations.[42,44] After 15 min at 9 °C, temperature was raised to 12 °C, which is above the L-L binodal. Figure 5e demonstrates that the dense liquid droplets forms at 10 and 9 °C rapidly dissociate. This cycle was repeated multiple times with identical evolution of the dense liquid droplets are each temperature.

In view of these four arguments, we conclude that the clusters do not represent a stable phase and their evolution observed in Figure 3 is a novel intriguing phenomenon in need of understanding. Toward this end, we first show that the clusters are in near-equilibrium with the solution and then, that heir evolution is akin to Ostwald ripening, with one significant discrepancy with the predictions for this process.

Clusters Are in Equilibrium with the Solution. Using the mean cluster size and the intensity of the light scattered by them we determine the concentration n_2 and volume fraction φ_2 of the clusters,[3,34] Figure 3c,d. At protein concentration 85 mg mL^{-1}, $n_2 \approx 10^{13}$ m^{-3}, which is near the detection limit of light scattering;[8] the n_2 and φ_2 data for this concentration have significant scatter and are not displayed. Integrating the size distributions determined by Brownian microscopy in Figure 2d, we find that the total concentration of clusters in a solution with C_1 = 100 mg mL^{-1} is $n_2 \approx 3 \times 10^{14}$ m^{-3}. This number is about 10× higher than n_2 evaluated from DLS data for a

dx.doi.org/10.1021/jp303316s | J. Phys. Chem. B 2012, 116, 10657–10664

solution with the same C_1 and at 24 h after preparation. This deviation is likely another consequence of the Rayleigh law: as demonstrated in refs 3 and 34 an overestimation of R_2 by a factor of x leads, at a given scattered intensity, to underestimating n_2 and φ_2 by factors of x^6 and x^3, respectively. We conclude that the n_2 data determined by light scattering and plotted in Figure 3c underestimate the actual values by ~10×, whereas those for φ_2 in Figure 3d, by ~3×.

To estimate the fraction of the protein in the clusters $\nu_2 = C_2\varphi_2/(C_1\varphi_1 + C_2\varphi_2)$, we assume that the protein concentration in the clusters C_2 is equal to that in a macroscopically stable dense liquid, C_2 = 450 mg mL^{-1},[28] which yields $\nu_2 \approx$ (2.25 to 5.3)φ_2/φ_1. In view of the underestimate of φ_2 discussed above, ν_2 is about 10× higher than the φ_2/φ_1 ratio plotted in Figure 3d. The values of φ_2/φ_1 in Figure 3d and the corresponding ν_2's are steady for 20 h for the 150 mg mL^{-1} solution and for 8 h for the 200 mg mL^{-1} solution, after which they increase by factors of 2.5 and 8, respectively.

To understand the increase of ν_2 at late times and the higher ν_2 at higher C_1, we characterize the thermodynamics of the tested solutions. We determine the osmotic compressibility $\partial\Pi/\partial C_1$ of the protein, which reflects the interactions between the lysozyme molecules. Figure 6a displays the concentration

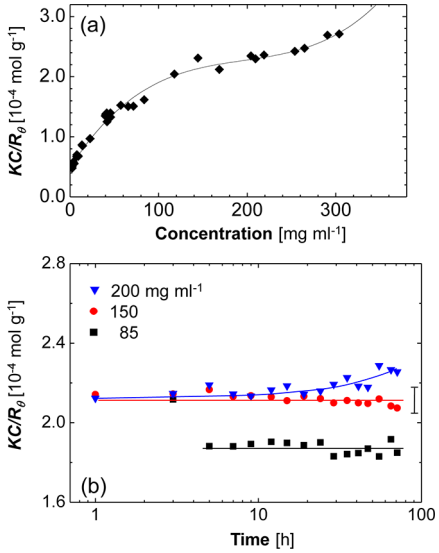

Figure 6. Interactions between the lysozyme molecules in the bulk solution characterized by the ratio KC_1/R_θ, where K is an instrument constant, C_1 is the concentration of lysozyme, and $R_\theta = I_\theta/I_0$ is the Raleigh ratio of the intensities of light scattered at angle θ = 90° and incident light. Only intensity scattered by monomers, obtained from the peak corresponding to monomers in the intensity distribution function, was considered in the determination of R_θ. (a) The dependence of KC_1/R_θ on C. (b) The evolution over 71 h, for three concentrations C_1 indicated in the plot. Error bar at 90 h in (b) indicates scatter of all data sets. Lines are just guides for the eye.

dependence of the ratio $KC_1/R_\theta = (N_A k_B T)^{-1}(\partial\Pi/\partial C_1)$, determined by static light scattering; the time-evolution of this ratio over 71 h at the three concentrations probed in Figure 3 is displayed in Figure 6b. The initial values of KC_1/R_θ in Figure 6b are equal to those at these three concentrations in Figure 6a. These values remain steady for the entire duration of the experiment at C_1 = 85 and 150 mg mL^{-1}. For C_1 = 200 mg mL^{-1}, KC_1/R_θ is steady for about 20 h but then increases. The KC_1/R_θ dependence on C_1 can be integrated to yield the chemical potential of the monomer μ_1 as discussed above and in ref 7: a steady KC_1/R_θ ratio indicates that μ_1 is steady for the period of monitoring, whereas an increasing KC_1/R_θ indicates that μ_1 increases. The increase of μ_1 at longer times is poorly understood and is a subject of ongoing investigation. This increase is not a sign of irreversible aggregation: as discussed above, the studied lysozyme solutions remain stable for several months and no amyloid formations are detected. It may involve partial protein unfolding and/or rearrangement of the water molecules and ions around the protein molecules. The decrease of the chemical potential of the water and ions associated with this rearrangement would compensate for the observed increase in μ_1.

Comparison of Figures 3d and 6b reveals a correlation between (i) the steady protein chemical potential μ_1 and the steady fraction of protein in the clusters ν_2 during the initial 20 and 8 h at 150 and 200 mg mL^{-1}, respectively, and (ii) the increasing μ_1 and ν_2 at later times at 200 mg mL^{-1}. The increase in KC_1/R_θ is weaker than the increase in ν_2 and φ_2/φ_1 and is not even visible at 150 mg mL^{-1}, where it may be hidden by the data scatter, see Figure 6b. Still, we conclude that the increase of ν_2 and φ_2/φ_1 at later times is due to the increase in μ_1.

To probe the correlation between ν_2 and C_1 we use the Gibbs distribution $\nu_2 \approx \exp(-\Delta g/k_B T)$, where Δg is the excess of the standard free energy of the protein in the clusters over that in the solution. Since $\nu_2 \approx 10\varphi_2/\varphi_1 = 7 \times 10^{-5}$ at 200 mg mL^{-1} and $\nu_2 \approx 3 \times 10^{-5}$ at 150 mg mL^{-1}, we find that Δg should decrease by about $k_B T$ as the concentration increases from 150 to 200 mg mL^{-1}. Furthermore, since that $\Delta g(C_1)$ is nearly linear, we extrapolate to find $\Delta g|_{150\text{mg/mL}}^{450\text{mg/mL}} \approx 6\ k_B T$. In ref 7 $\Delta g(C_1)$ was evaluated from the osmotic compressibility data as in Figure 6a. Both of the above estimates of Δg are in prefect agreement with that evaluation.

The correlations between ν_2 and μ_1 and Δg lead to two important conclusions: (i) Cluster formation is a reversible process, and the clusters are in near equilibrium with the solution, up to a capillary correction, as discussed below. (ii) The fraction of protein molecules sequestered in the clusters is determined by the excess of standard free energy (i.e., the concentration-independent part of the bulk free energy) of the cluster phase over that of the solution.

Mechanism of Cluster Maturation. Toward understanding of the microscopic mechanism of the maturation of the cluster population reflected by the data in Figures 2 and 3, we note that the growth of the average cluster size at a steady cluster volume fraction indicates that bigger clusters grow at the expense of smaller ones. This evolution is formally similar to Ostwald ripening of new phases whereby molecules "evaporate" from small domains of a minority phase (which, due to their higher surface free energy, are supersaturated with respect to the solution) and "condense" on larger domains, which have lower surface free energy and are undersaturated.[24] Ostwald ripening is a common phenomenon in materials production by solidification or precipitation.[38,45,46] Ostwald ripening of droplets of protein dense liquid stable with respect to the tested solutions (and metastable with respect to the crystal phase) has been observed before.[42,47]

The cluster evolution in Figure 3 has several features in common with the Lifshitz–Slyozov–Wagner (LSW) scenario of Ostwald ripening.[22,23] (i) The LSW scenario predicts that the minority phase domains grow with time as $t^{1/3}$;[22] subsequent nonmean field treatments yield a somewhat lower exponent.[48] The $t^{0.26}$ law in Figure 3a complies with this

prediction. (ii) The domain size is independent of the concentration of the majority phase and the minority phase volume fraction, see eq 28 of ref 22, in agreement with the data in Figure 3a. (iii) The domain size distribution during ripening is characterized by a single length scale.[22] Figure 3b displays the width σ_2 of the cluster peak in the distribution functions determined independently of R_2 (which was possible only for the 200 mg mL^{-1} solution). This σ_2 is proportional to R_2, i.e., the size distribution is scale-invariant. Figure 3a also shows that the scale-invariant LSW expression for the cluster size distribution (eq (24) of ref 22) is compatible with the present cluster size distribution. Despite these three common features, application of the prediction of the LSW kinetic law to the present system yields a cluster growth rate that is at least an order of magnitude greater than the observed value; see evaluation in the Supporting Information.

Another mechanism of ripening in liquid two-phase systems, by coalescence of new phase domains, was put forth by Binder, Stauffer, and Siggia.[49,50] This mechanism would also lead to a $t^{1/3}$-like growth of the average cluster size, at a scale invariant cluster size distribution. In contrast to the LSW scenario, since the rate of coalescence depends on the concentration of the domains, the domain size scales with the amount of minority phase. The data in Figure 3 contradict this scaling: while φ_2 varies between 2×10^{-8} (at 85 mg mL^{-1}) and 7×10^{-6} (at 71 h at 200 mg mL^{-1}), the cluster sizes R_2 follow a unique time dependence. Correspondingly, Supporting Movie 1 demonstrates that no cluster collisions or coalescence occur for 30 s of cluster evolution monitored by Brownian microscopy. As discussed in the Supporting Information, the likely reason for the low contribution of coalescence to the cluster growth is the low volume fraction of the clusters.[50]

Finally, if the clusters' growth rate were limited by the kinetics of association of incoming molecules at the cluster interface, one would observe $R_2 \propto t^{1/2}$;[23] hence, this mechanism can be dismissed as well.

The above comparisons between the predictions of the three mechanisms and the data on cluster evolution suggest that cluster growth occurs by a mechanism similar to the LSW scenario of Ostwald ripening, i.e., by exchange of single molecules between clusters, driven by the minimization of the total surface free energy of the cluster population. A 10-fold discrepancy between the observed cluster growth rate and the LSW prediction is not uncommon in the studies of Ostwald ripening in classical materials systems.[38,45,46] In the Supporting Information, we discuss three known mechanisms that may lead to this discrepancy: (i) Overlapping of the diffusion supply fields of growing clusters, which may slow down individual cluster growth.[45] (ii) Variations in the shape of the initial cluster size distribution.[38,46] (iii) A second-order chemical reaction which is the rate limiting step in the cluster growth mechanism.[45] We show that only mechanism (ii) does not contradict the observations about cluster behavior in Figure 3 and might be applicable to the observed clusters evolution.

In addition to these, we propose another qualitative explanation of slower growth of the clusters: it may stem from the cluster composition of mostly protein complexes of limited lifetime, demonstrated in ref 7. Thus, the flux from smaller to larger clusters is affected by the dynamics of formation of the transient complexes at the cluster interface and their decay to monomers in the solution.

Further evaluation of the reasons for the slow rate of cluster growth is work in progress.

CONCLUSIONS

We have shown that the anomalous mesoscopic clusters in solutions of the protein lysozyme are in equilibrium with the solution. This indicates, importantly, that cluster formation is a reversible process.

We have demonstrated that the size of the clusters increases following a universal power law, independent of the protein concentration and cluster volume fraction. The cluster size distribution retains a scale-invariant shape during growth. These observations indicate the action of a mechanism akin to the Lifshitz−Slyozov-Wagner mechanism of Ostwald ripening. It is surprising that this mechanism proposed for stable phases applies to the anomalous clusters, whose existence contradicts the classical understanding of phases and phase equilibria. In view of the role of the anomalous mesoscopic clusters as nucleation sites for crystals and other ordered solid aggregates, the cluster evolution may explain several mysteries of nucleation: increasing nucleation rates under steady external conditions, conucleation of polymorphs, and others.

The cluster size is ∼10× smaller than predicted by the LSW theory. Such discrepancy is not uncommon in studies of new-phase coarsening. Its detailed explanation is the subject of ongoing cluster work.

ASSOCIATED CONTENT

Supporting Information

Details about the characterization of the size and volume fraction of the clusters from the dynamic light scattering data and a discussion of two mechanisms of cluster ripening: by the exchange of single molecules and by coalescence. This material is available free of charge via the Internet at http://pubs.acs.org.

AUTHOR INFORMATION

Corresponding Author

*E-mail: vekilov@uh.edu. Tel: 1-713-743-4315. Fax: 1-713-743-4323.

Notes

The authors declare no competing financial interest.

ACKNOWLEDGMENTS

We thank J. Cabiness from Nanosight Ltd. for kindly providing a Nanosight device used in the Brownian microscopy characterization of the clusters and W. Pan for help with the experimental methods and for obtaining preliminary data. This work is supported by the National Science Foundation (Grant MCB-0843726 to V.L. and P.G.V.), and The Norman Hackerman Advanced Research Program (Grant 003652-0078-2009 to P.G.V.). V.L. is supported in part by the Arnold and Mabel Beckman Foundation Beckman Young Investigator Award, the Alfred P. Sloan Research Fellowship, and The Welch Foundation through Grant E-1765.

REFERENCES

(1) Gliko, O.; Neumaier, N.; Pan, W.; Haase, I.; Fischer, M.; Bacher, A.; Weinkauf, S.; Vekilov, P. G. *J. Am. Chem. Soc.* **2005**, *127*, 3433−3438.

(2) Gliko, O.; Pan, W.; Katsonis, P.; Neumaier, N.; Galkin, O.; Weinkauf, S.; Vekilov, P. G. *J. Phys. Chem. B* **2007**, *111*, 3106−3114.

(3) Pan, W.; Galkin, O.; Filobelo, L.; Nagel, R. L.; Vekilov, P. G. *Biophys. J.* **2007**, *92*, 267−277.

(4) Uzunova, V. V.; Pan, W.; Galkin, O.; Vekilov, P. G. *Biophys. J.* **2010**, *99*, 1976−1985.

(5) Knee, K. M.; Mukerji, I. *Biochemistry* **2009**, *48*, 9903−9911.

(6) Georgalis, Y.; Umbach, P.; Saenger, W.; Ihmels, B.; Soumpasis, D. M. *J. Am. Chem. Soc.* **1999**, *121*, 1627−1635.
(7) Pan, W.; Vekilov, P. G.; Lubchenko, V. *J. Phys. Chem. B* **2010**, *114*, 7620−7630.
(8) Vekilov, P. G.; Pan, W.; Gliko, O.; Katsonis, P.; Galkin, O. Metastable mesoscopic phases in concentrated protein solutions. In *Lecture Notes in Physics, Vol. 752: Aspects of Physical Biology: Biological Water, Protein Solutions, Transport and Replication*; Franzese, G., Rubi, M., Eds.; Springer: Heidelberg, 2008; pp 65−95.
(9) Galkin, O.; Pan, W.; Filobelo, L.; Hirsch, R. E.; Nagel, R. L.; Vekilov, P. G. *Biophys. J.* **2007**, *93*, 902−913.
(10) Vekilov, P. G. *Cryst. Growth Des.* **2010**, *10*, 5007−5019.
(11) Brubaker, W. D.; Freites, J. A.; Golchert, K. J.; Shapiro, R. A.; Morikis, V.; Tobias, D. J.; Martin, R. W. *Biophys. J.* **2011**, *100*, 498−506.
(12) Pouget, E. M.; Bomans, P. H. H.; Goos, J. A. C. M.; Frederik, P. M.; de With, G.; Sommerdijk, N. A. J. M. *Science* **2009**, *323*, 1455−1458.
(13) Gebauer, D.; Volkel, A.; Colfen, H. *Science* **2008**, *322*, 1819−1822.
(14) Gower, L. B. *Chem. Rev.* **2008**, *108*, 4551−4627.
(15) Erdemir, D.; Lee, A. Y.; Myerson, A. S. *Acc. Chem. Res.* **2009**, *42*, 621−629.
(16) Aber, J. E.; Arnold, S.; Garetz, B. A. *Phys. Rev. Lett.* **2005**, *94*, 145503.
(17) Wang, J. F.; Muller, M.; Wang, Z. G. *J. Chem. Phys.* **2009**, 130.
(18) Leunissen, M. E.; Christova, C. G.; Hynninen, A.-P.; Royall, C. P.; Campbell, A. I.; Imhof, A.; Dijkstra, M.; van Roij, R.; van Blaaderen, A. *Nature* **2005**, *437*, 235−240.
(19) Savage, J. R.; Dinsmore, A. D. *Phys. Rev. Lett.* **2009**, *102*, 198302.
(20) Zhang, T. H.; Liu, X. Y. *J. Phys. Chem. B* **2007**, *111*, 14001−14005.
(21) Hutchens, S. B.; Wang, Z.-G. *J. Chem. Phys.* **2007**, *127*, 084912.
(22) Lifshitz, I. M.; Slyozov, V. V. *J. Phys. Chem. Solids* **1961**, *19*, 35−50.
(23) Wagner, C. *Elektrochem* **1961**, 65.
(24) Ostwald, W. *Lehrbuch der Allgemeinen Chemie* Leipzig, Germany, **1896**; Vol. *2*.
(25) Thomas, B. R.; Vekilov, P. G.; Rosenberger, F. *Acta Crystallogr. Sect. D* **1996**, *52*, 776−784.
(26) Vekilov, P. G.; Monaco, L. A.; Thomas, B. R.; Stojanoff, V.; Rosenberger, F. *Acta Crystallogr. Sect. D* **1996**, *52*, 785−798.
(27) Galkin, O.; Vekilov, P. G. *J. Phys. Chem.* **1999**, *103*, 10965−10971.
(28) Petsev, D. N.; Wu, X.; Galkin, O.; Vekilov, P. G. *J. Phys. Chem. B* **2003**, *107*, 3921−3926.
(29) Filobelo, L. F.; Galkin, O.; Vekilov, P. G. *J. Chem. Phys.* **2005**, *123*, 014904.
(30) Eisenberg, D.; Crothers, D. *Physical Chemistry with Applications to Life Sciences*; The Benjamin/Cummins: Menlo Park, 1979.
(31) Lide, D. R. *CRC Handbook of Chemistry and Physics*; Taylor and Francis: London, 2004.
(32) Petsev, D. N.; Thomas, B. R.; Yau, S.-T.; Vekilov, P. G. *Biophys. J.* **2000**, *78*, 2060−2069.
(33) Provencher, S. W. *Comput. Phys. Commun.* **1982**, *27*, 229−242.
(34) Li, Y.; Lubchenko, V.; Vekilov, P. G. *Rev. Sci. Instrum.* **2011**, *82*, 053106.
(35) Mikol, V.; Hirsch, E.; Giege, R. *J. Mol. Biol.* **1990**, *213*, 187−195.
(36) Muschol, M.; Rosenberger, F. *J. Chem. Phys.* **1995**, *103*, 10424−10432.
(37) Russel, W. B. *Annu. Rev. Fluid Mech.* **1981**, *13*, 425−455.
(38) Chen, M. K.; Voorhees, P. W. *Modell. Simul. Mater. Sci. Eng.* **1993**, *1*, 591−612.
(39) Steinrauf, L. K. *Acta Crystallogr.* **1959**, *12*, 77−78.
(40) Lomakin, A.; Chung, D. S.; Benedek, G. B.; Kirschner, D. A.; Teplow, D. B. *Proc. Natl. Acad. Sci. U.S.A.* **1996**, *93*, 1125−1129.
(41) Filobelo, L. Kinetics of Phase Transition in Protein Solutions on Microscopic and Mesoscopic Length Scales, PhD Disseration, University of Houston, December 2005.
(42) Shah, M.; Galkin, O.; Vekilov, P. G. *J. Chem. Phys.* **2004**, *121*, 7505−7512.
(43) Galkin, O.; Vekilov, P. G. *Proc. Natl. Acad. Sci. U.S.A.* **2000**, *97*, 6277−6281.
(44) Shah, M.; Galkin, O.; Vekilov, P. G. *J. Phys. Chem. B* **2009**, *113*, 7340−7346.
(45) Kahlweit, M. *Adv. Colloid Interface Sci.* **1975**, *5*, 1−35.
(46) Thornton, K.; Akaiwa, N.; Voorhees, P. W. *Phys. Rev. Lett.* **2001**, *86*, 1259−1262.
(47) Streets, A. M.; Quake, S. R. *Phys. Rev. Lett.* **2010**, 104.
(48) Langer, J. S.; Schwartz, A. J. *Phys. Rev. A* **1980**, *21*, 948−958.
(49) Binder, K.; Stauffer, D. *Phys. Rev. Lett.* **1974**, *33*, 1006.
(50) Siggia, E. D. *Phys. Rev. A* **1979**, *20*, 595−605.